frontiers | Frontiers in Earth Science

TYPE Original Research
PUBLISHED 11 December 2025
DOI 10.3389/feart.2025.1658491

OPEN ACCESS

EDITED BY
Summer Rupper,
The University of Utah, United States

REVIEWED BY
Seweryn Lipiński,
University of Warmia and Mazury in Olsztyn, Poland
Degang Zhou,
Chinese Academy of Sciences (CAS), China
Nilamoni Barman,
Central Ground Water Board, India

*CORRESPONDENCE
Rebecca Mott,
mott@slf.ch

RECEIVED 02 July 2025
REVISED 18 November 2025
ACCEPTED 27 November 2025
PUBLISHED 11 December 2025

CITATION
Mott R, Haugeneder M, Stiperski I, Asemann P, Reynolds D and Nicholson L (2025) Characterization of the near-surface air temperature dynamics over glaciers using thermal infrared measurements. *Front. Earth Sci.* 13:1658491. doi: 10.3389/feart.2025.1658491

Characterization of the near-surface air temperature dynamics over glaciers using thermal infrared measurements

Rebecca Mott[1]*, Michael Haugeneder[1], Ivana Stiperski[2], Patricia Asemann[1,3], Dylan Reynolds[3] and Lindsey Nicholson[2]

[1]WSL Institute for Snow and Avalanche Research SLF, Davos, Switzerland, [2]Department of Atmospheric and Cryospheric Sciences, University of Innsbruck, Innsbruck, Austria, [3]School of Architecture, Civil and Environmental Engineering, Ècole Polytechnique Fèdèrale de Lausanne, Lausanne, Switzerland

Alpine glaciers are undergoing rapid mass loss, primarily driven by rising summer air temperatures. However, the glacier microclimate, especially the role of atmospheric dynamics near the surface and turbulent fluxes, is not adequately understood. This study examines the structure and variability of the glacier boundary layer, focusing on katabatic winds and their modulation by synoptic-scale disturbances. Using a high-resolution thermal infrared (TIR) camera (InfraTec VarioCam HD) directed at synthetic screens, we recorded spatio-temporally resolved air temperature fields within the lowest 4 m above the glacier surface. These measurements were complemented by turbulence data from a 5-m eddy covariance tower, enabling a combined analysis of thermal stratification and turbulent mixing. Our results reveal persistent temperature stratification during katabatic flow, often marked by strong gradients and localized zones of high temperature variance associated with the katabatic jet. These layers are intermittently disrupted by cross-glacier or synoptic-scale flows, enhancing turbulent mixing and advecting warm air toward the surface. The height of maximum temperature variance frequently coincided with the approximate jet height estimated from turbulence measurements, suggesting a link between glacier wind dynamics and thermal structure. However, this relationship weakens under fluctuating flow regimes, highlighting the complexity of glacier boundary layer processes and suggesting that stratification and mixing are highly sensitive to the vertical structure of glacier winds. The use of TIR imaging offers unique insights into the fine-scale temperature dynamics of glacier boundary layers, overcoming limitations of discrete-level turbulence sensors and enabling continuous spatial assessment of flow features. Our findings underscore the importance of shallow katabatic winds in enhancing near-surface mixing, with implications for the surface energy balance and, ultimately, glacier melt. Future research should combine this approach with advanced heat budget models and adapted methods such as the WEIRD technique to further unravel the complex coupling between glacier winds, atmospheric turbulence, and climate sensitivity of mountain glaciers.

KEYWORDS

glacier wind, jet height, thermal infrared (TIR) camera, heat exchange processes, thermodynamics, atmospheric turbulence

1 Introduction

Ongoing mass changes of Alpine glaciers are dramatic, mainly driven by rising air temperatures in summer. To further predict future glacier mass changes, we have to understand the climatic drivers of the glacier, the microclimate of glaciers, and the sensitivity of the glacier microclimate to a warming climate. Examining processes occurring at the interface between glaciers and the atmosphere is therefore critical, as they profoundly influence the glacier's surface energy balance and catchment hydrology. This underscores the need for more advanced models and experimental methods which resolve these intricate factors to comprehensively understand glacier dynamics.

A mountain glacier's mass balance is influenced by the interplay of energy, mass, and momentum fluxes at the glacier-atmosphere interface (e.g., Fitzpatrick et al., 2017). While radiation primarily contributes to melt energy (Hock, 2005), turbulent fluxes emerge as significant, particularly during intense melt events over shorter time frames (Fitzpatrick et al., 2017; Brock et al., 2007). These turbulent fluxes constitute a substantial portion, ranging from 35%–50%, of the glacier surface energy balance (SEB), with their impact intensifying under cloudy and windy conditions (Chambers et al., 2021; Conway and Cullen, 2013; Conway et al., 2022). Therefore, a comprehensive understanding of turbulent fluxes is paramount for accurately predicting how glaciers respond to evolving climatic conditions.

The glacier boundary layer is characterized by downslope glacier winds, commonly called katabatic winds or glacier winds. These glacier winds result from flux divergence driven by the difference in air temperature between the often stably stratified cooler atmospheric layer near the surface and the warmer surrounding air (Sauter et al., 2025). These flux divergences not only drive the glacier wind, but also contribute to the melting of the glacier surface.

Glacier winds play a crucial role in turbulent exchange processes and act as a barrier, shielding the glacier surface from synoptic-scale warm air advection (Smeets et al., 2000; Oerlemans, 2001; Sauter et al., 2025). Moreover, katabatic winds extend their influence beyond glaciers to perennial ice fields, impacting local weather (Mott et al., 2019). A semi-idealized modeling approach by Sauter and Galos (2016) revealed that the intricate interplay between local katabatic winds, synoptic winds, and topography significantly modulates turbulent fluxes of sensible heat over glaciers.

Recent experimental research by Mott et al. (2020) highlighted the significant role of synoptic-scale motions in disrupting katabatic winds and changing thermodynamics over the glacier surface. Turbulence measurements showed that synoptic winds can disrupt prevailing katabatic flows, generating across-glacier winds and warm-air advection from surrounding ice-free areas. These events increase near-surface air temperatures and horizontal temperature gradients, enhancing turbulent heat exchange over the glacier center while sheltered peripheral zones remain more stably stratified. This disruption leads to intense turbulent mixing and subsequent heat advection toward the near-glacier surface, consequently altering the near-surface air temperature. These mechanisms were also corroborated in the Large Eddy Simulations (LES) complementing the experimental work by Goger et al. (2022) and Goger et al. (2025).

Both studies underscored the pivotal role of glacier winds in shaping the glacier microclimate, which can either exacerbate or alleviate glaciers' vulnerability to rising air temperatures (Hoinkes, 1954; Mott et al., 2020; Shaw et al., 2023). Despite these recent advancements in experimental and numerical research, the mechanisms governing the coupling between the glacier boundary layer and synoptic flow, along with their implications for the total mass balance of glaciers, remain predominantly unresolved. Crucially, advancement in this area is hampered by the limited ability of both field observations and even the highest resolution models to capture the appropriate scales of exchange in the glacier boundary layer. Experimental investigations into glacier microclimates frequently suffer from a lack of detailed data concerning heat exchange processes and temperature dynamics in close proximity to the glacier surface (lowest meter above the surface) (Mott et al., 2020). To understand the impact of spatiotemporal variations in atmospheric flow over glaciers on their microclimate, highly resolved atmospheric data, both temporally and spatially, is imperative. Such data is essential for elucidating the intricate mechanisms of the glacier microclimate dynamics and for validating the emerging state-of-the-art high-resolution atmospheric models.

We utilized thermal imaging to analyze the dynamics and stratification of the near-surface atmospheric layer above the glacier. Our setup employed a high-resolution thermal infrared (TIR) camera (InfraTec VarioCam HD) directed towards synthetic screens. Previous studies have demonstrated the effectiveness of this method in examining slope flows (Grudzielanek and Cermak, 2015) and temperature dynamics over patchy snow covers (Haugeneder et al., 2023; 2024). Our study aims to explore its applicability in studying near-surface air temperature dynamics within glacier winds. Specifically, we seek to characterize the temperature variations in close proximity to the glacier surface. To this end, we investigated the near-surface temperature response during purely katabatic flows and disturbed flow conditions.

Despite capturing only temperature, TIR imaging offers valuable insights into glacier boundary layer dynamics due to the tight coupling of turbulent variables in stably stratified, katabatic flows, where temperature structures can indirectly reflect key dynamical features. Models (Denby, 1999)and observations (Grachev et al., 2016) suggest that the height of the katabatic jet often coincides with a maximum in potential temperature variance. While this jet maximum height is difficult to resolve accurately with discrete-level eddy covariance measurements, high-resolution TIR data allow for a more continuous assessment of its position and variability.

2 Methods

2.1 Study area

The Hintereisferner (HEF) is a valley glacier located in the Ötztal Alps, Austria. HEF is recognized as one of the "reference glaciers" by the World Glacier Monitoring Service. Since 1952/53, ongoing observations form part of a comprehensive catchment monitoring program (Strasser et al., 2018). HEF has played a crucial role as a testbed for developing instruments, methods,

and models (Kuhn et al., 1999) and exploring glacier and valley winds (Obleitner, 1994).

Building on this legacy, the Hintereisferner Experiment (HEFEX I) micrometeorological measurement campaign unfolded over 3 weeks in August 2018 (Mott et al., 2020). Subsequently, the more extensive HEFEX II campaign took place in August 2023, aiming to delve into the glacier's microclimate through a combination of an extensive network of meteorological stations and various remote sensing measurements (Nicholson et al., 2025).

Hintereisferner, a classical valley glacier, measured approximately 6.3 km in length in 2018, with an elevation difference of around 1,200 m (https://wgms.ch/, last access: 11 December 2020). The glacier is nestled in a northeast-oriented valley with steep slopes. Positioned in the "inner dry Alpine zone" (Frei and Schär, 1998), one of the driest regions in the European Alps, Hintereisferner has undergone significant shrinkage in recent decades, with a 15% decrease in glacier area recorded between 2001 and 2011 (Klug et al., 2018; Abermann, 2009).

2.2 Thermal infrared measurements

In this study, we used an InfraTec VarioCAM HD thermal infrared camera with a spatial resolution of 1,024 × 768 pixels to monitor air temperature dynamics near the glacier surface. The camera was aimed at two vertically mounted screens made from a thin, stretched polyester mat coated with acrylate (Haugeneder et al., 2023). Due to the material's ability to rapidly equilibrate with ambient air temperature, we assume that its surface temperature provides a reliable proxy for air temperature. Following Grudzielanek and Cermak (2015), the emissivity of the screen material is taken as 0.94.

The screens were precisely aligned with the direction of the glacier wind (Figure 1c). These screens were strategically configured to facilitate the measurement of flow patterns and the corresponding temperature dynamics along the primary wind direction. The camera was positioned so that the screen is parallel to the glacier surface. In addition, they allowed for the assessment of the vertical profiles of air temperature below and above the height of the katabatic jet. Data on turbulence gathered during a previous measurement campaign in 2018 (HEFEX I) indicates that a jet typically forms between 1.7 and 2.3 m above the ice surface under katabatic-flow conditions. Screen 1, with dimensions of 1.9 m in height and 3 m in length, was utilized to measure along-flow patterns. Screen 2, measuring 3.8 m in height and 1.9 m in width, captured the vertical temperature profile. As this study focuses on temperature dynamics along the vertical profile in conjunction with station data, the analysis was restricted to Screen 2. Given the distance of the IR camera to the screen, the horizontal and vertical resolution is 6.1 mm/pixel and 5.8 mm/pixel respectively. The TIR camera captured infrared frames at a rate of 30 Hz. To account for slight variations in material thickness and the sensitivity of screen emissivity to minor surface contamination, we adopted the method of Grudzielanek and Cermak (2015), averaging TIR values across 10 horizontal pixels along the vertical profile to enhance the reliability of the temperature measurements. Furthermore, the measurements may be influenced by solar heating of the material, depending on the sun's angle. As a result, absolute temperatures obtained from daytime TIR measurements can exhibit a positive bias. To address this, it is recommended to focus on relative temperature changes over space or time rather than relying on absolute values (Haugeneder et al., 2023).

While the full HEFEX II campaign was running over 3 weeks in August 2023, thermal infrared measurements were only conducted during the Intensive Observation Period (IOP), lasting 3 days (August 22–24) (Nicholson et al., 2025). Due to the substantial volume of data storage required, the measurements were not carried out continuously but were confined to sequences lasting from 1 hour to several hours during the day and night. For this study, we've chosen five compelling sequences during August 22 and 23 to demonstrate the efficacy of our method in characterizing the spatial and temporal temperature dynamics of glacier winds. These sequences illustrate its ability to capture temperature fluctuations during purely katabatic diurnal and nocturnal flows and disturbed situations throughout the day and night at an ultra-high resolution. Combining the TIR data with turbulence data from the near-by tower further allows an analysis of the approximate jet height location.

2.3 Automatic weather stations

Meteorological conditions and turbulence were measured using a 5-m weather tower (T275) with various sensors installed at different vertical levels (Figures 1a,b) (Nicholson et al., 2025). Low-frequency 2D wind speed and direction (Young JR 04101) was measured at 5.5 m. Unventilated Low-frequency temperature and humidity sensors (HC2A-S3 Rotronic) were placed at the 2.2 and 4.2 m levels. Low-frequency measurements were sampled every minute and averaged to 10 min intervals. A pressure sensor (CS100 Campbell Scientific) was located in the logger box. Furthermore, the station was equipped with one IRGASON and two 3D sonic anemometers (CSAT3) at 1.1, 2.0, and 4.0 m, respectively. The station was positioned close to the IR measurement setup at the glacier centerline (Figure 1).

Turbulence statistics from this tower at 1.1, 2 and 4 m above the surface were processed using 1 min averages (as suggested by the multi-resolution flux decomposition, Vickers and Mahrt, 2003) with prior linear detrending. Double rotation was used to rotate the data into the streamline coordinates, so that the u refers to the longitudinal, v lateral and w surface-normal velocity component (*cf.* Mott et al., 2020).

3 Results and discussion

3.1 Meteorological conditions measured at automatic weather station

We selected five periods during the IOP characterized by two different wind systems (*cf.* Mott et al., 2020): (i) purely katabatic conditions with a persistent flow direction from the southwest (defined as 200° at meteorological station T275) and wind velocities greater than 3 m/s (periods P1, P5 in Figure 2); (ii) disturbed flow conditions with wind directions deviating by more than 60° but less than 120° from the dominant katabatic-flow direction, indicating

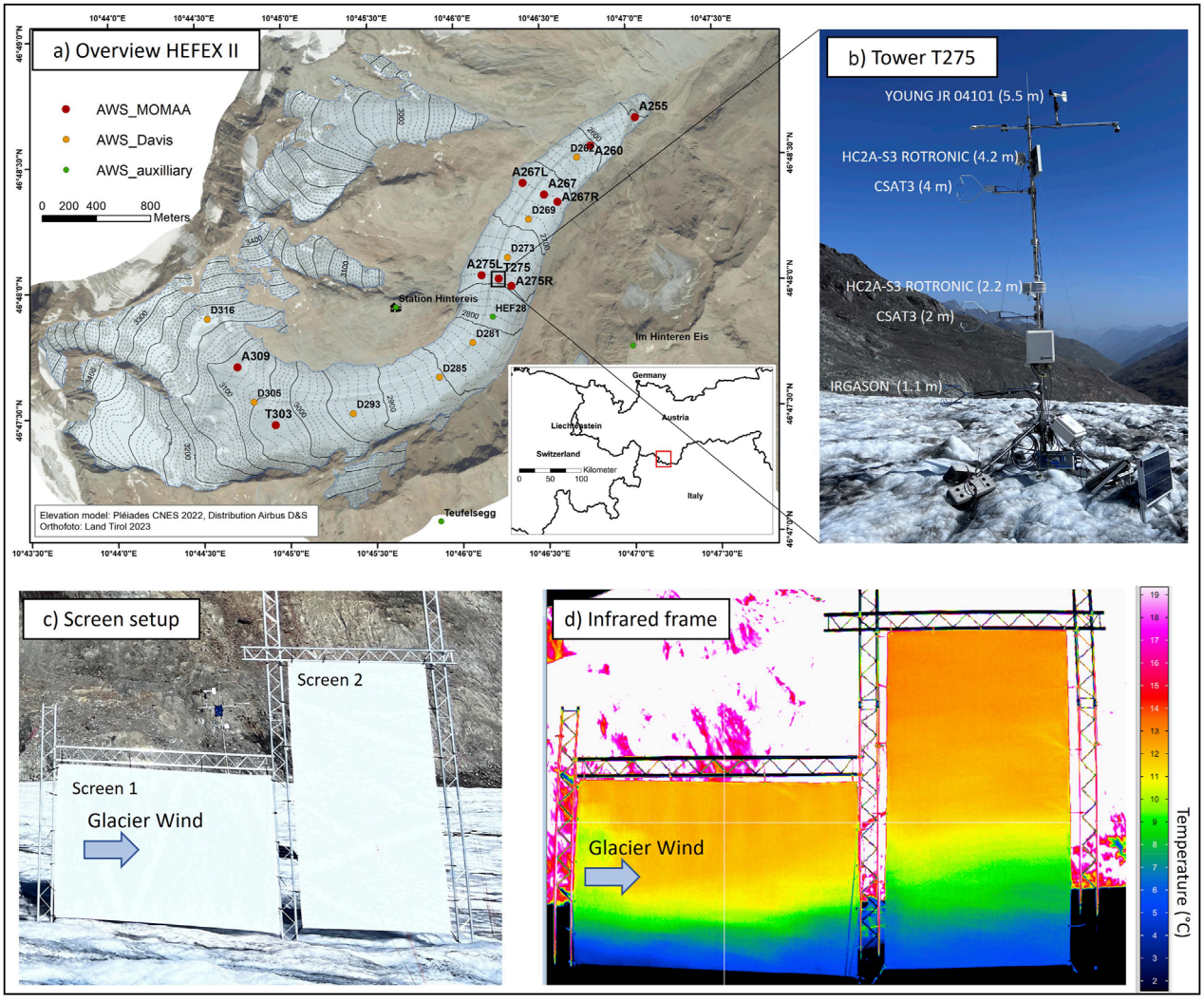

FIGURE 1
Overview of the HEFEX II campaign and measurement setup: **(a)** Map of the HEFEX II campaign (adapted from (Nicholson et al., 2025)) with the black rectangle highlighting the experimental setup used for this study; **(b)** the 5-m weather tower T275; **(c)** general view of the screen setup; **(d)** example of an infrared screen snapshot illustrating the surface temperature, used as a proxy for air temperature.

across-glacier winds (P3, P4) (Figure 2). While P3 exhibits a southwesterly across-glacier wind with strong disturbances, P4 is characterized by a northeasterly across-glacier wind, interspersed with short phases of glacier winds. During P2, a slight southerly flow with lower wind speeds occasionally disturbed the down-glacier wind. These conditions are typical at Hintereisferner, as discussed by Mott et al. (2020). They could show that these flows across the glacier measured at the glacier were associated with strong heat advection with the larger-scale flow. A significant increase in near-surface air temperature indicated horizontal heat advection.

During down-glacier wind conditions (P1, P2, P5), measurements revealed that wind speeds were highest at the 1.1 m and 2 m levels and consistently lower at the 4 m level, indicating that the jet maximum was located below 4 m. Additionally, temperatures were lower at the lower sensors, with more pronounced temperature gradients near the surface.

Despite generally lower near-surface wind speeds during across-glacier flows (P3, P4), downward turbulent heat fluxes were similar to or even higher than those observed during down-glacier winds caused by increased air temperatures during these periods (as already demonstrated in Mott et al., 2020). In the early morning katabatic flow conditions (P1), the highest downward (most negative) sensible heat fluxes occurred at the lowest measurement level. However, by late morning (P2), the two upper measurement levels exhibited more downward (negative) heat fluxes.

No clear relationship was observed at night between the magnitude of downward sensible heat fluxes and measurement height. Under disturbed flow conditions, air temperature and wind speed became much more uniform across the three measurement levels, suggesting less stable atmospheric stratification.

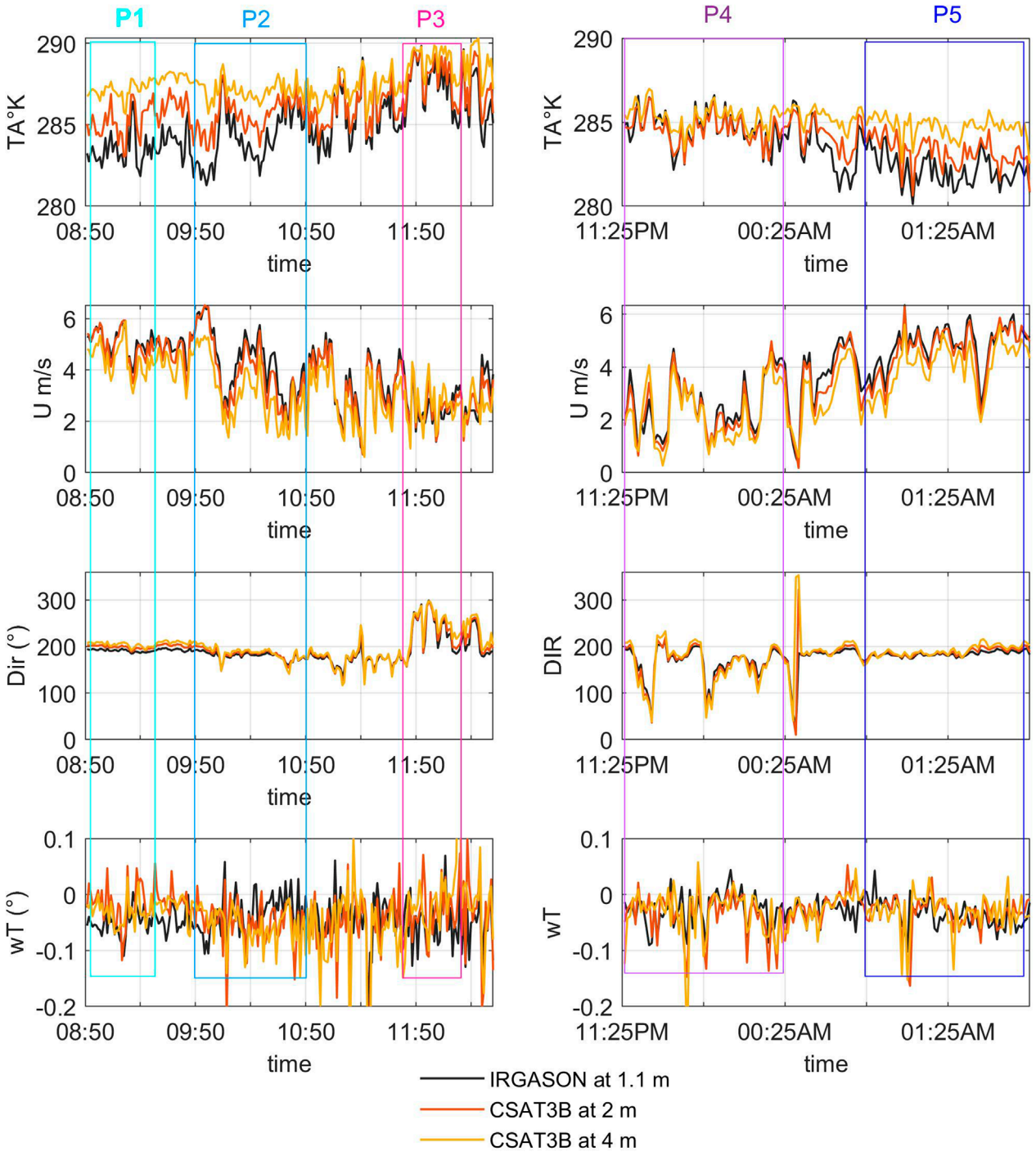

FIGURE 2
Virtual air temperature (TA), wind speed (U), wind direction (Dir), and kinematic turbulent sensible heat flux were measured using IRGASON and CSAT3B sensors at three heights (1.1 m, 2 m, and 4 m) above the glacier surface. Data were averaged over 1-min intervals on August 22–23, 2023. The periods selected for further analysis, P1–P5, are highlighted with boxes. Note that P1–P3 correspond to daytime periods, while P4 and P5 represent nighttime periods.

3.2 Validation of TIR data with station data: comparison of mean temperatures, gradients, variance and spectra

Daytime TIR measurements can be affected by solar heating of the screen material, depending on the sun's angle. Similarly, conventional temperature sensors are also prone to solar radiation effects. To assess the consistency between different temperature measurement methods, we compared air temperature readings from the station with those derived from the TIR camera. Specifically, we used low-frequency (10-min interval) data from unventilated ROTRONIC sensors at heights of 2.2 m and 4.2 m,

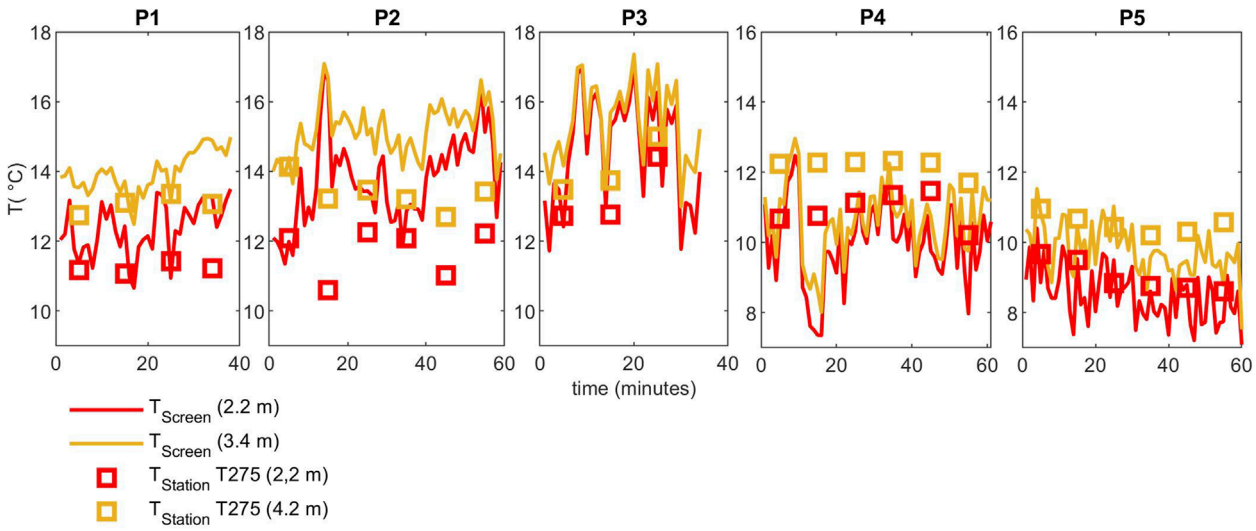

FIGURE 3
Time series of 1-min averaged temperatures measured at the screen at 2.2 m and 3.4 m above ground, compared with 10-min instantaneous air temperature measurements from low-frequency sensors at 2.2 m and 4.2 m above ground at T275.

and compared them to 1-min averaged temperatures obtained from the TIR camera at 2.2 m and at the screen's highest measurement point of 3.4 m (Figure 3). Since thermal stratification is essential for turbulent heat fluxes, temperature gradients between the first and second measurement level (L1) and the second and third measurement level (L2) are compared between the screen measurements, the fast response sensors (L1 and L2, Irgasons and CSAT) and the low response sensors (only available for L2) (Figure 4). The comparison between high-frequency and low-frequency (instantaneous) measurements, indicated by single points, aims to assess whether the different methods capture a similar range of temperatures. Although the techniques are not directly comparable—the upper measurement heights differ by 0.8 m between screen and tower, and the screen and tower are located approximately 15 m apart horizontally—this comparison provides a general sense of agreement between the datasets. Screen temperatures are corrected for the estimated emissivity of the screen material following the methodology suggested by Grudzielanek and Cermak (2015).

A comparison of the two upper-level temperature measurements reveals distinct differences between daytime and nighttime conditions (Figure 3). During the day, low-frequency sensors record slightly lower temperatures—particularly in period P2—while measurements align well in periods P1 and P3. At night, when shortwave radiation errors are minimal, low-frequency sensors register higher temperatures during period P4, coinciding with a disturbance in the glacier wind. In contrast, temperature measurements at both levels show good agreement during the katabatic glacier wind event in period P5. Overall, the bias between screen temperatures and low-response sensor temperatures is 0.67 °C at measurement level S2 (2.2 m) and 0.48 °C at S3 during katabatic conditions (Table 1), and −0.10 °C at S2 and -0.57 °C at S3 (4.2 m) during disturbed wind conditions. When separated into daytime and nighttime conditions, the temperature biases exhibit a clear contrast: nighttime biases are −0.7 °C and −1.2 °C, whereas daytime biases rise to 1.5 °C and 1.4 °C. The positive daytime biases suggest that the screen temperatures were influenced by shortwave solar radiation, with the magnitude of this effect depending on the solar angle of incidence. This influence was particularly evident during period P2, which showed a stronger positive temperature offset, likely due to enhanced direct solar exposure of the screen. Additionally, lower wind speeds during P2 compared to P1 may have amplified the solar heating effect by reducing convective cooling of the screen material. Conversely, the negative nighttime biases likely reflect radiative longwave cooling of the screen surface. This comparison further highlights the importance of collocated high-frequency air temperature measurements—such as those obtained from fine-wire thermocouples—to accurately validate absolute screen temperatures.

Temperature gradient comparisons (Figure 4) indicate that TIR measurements at the screen closely match those from the fast-response sensors—especially at the upper level—where gradient biases range between 0.05 °C and 0.3 °C per meter. During period P4, fast-response sensor readings at L1 indicate unstable atmospheric conditions, whereas all other instruments, including the screen, suggest slightly stable conditions, reflected in mildly positive temperature gradients. The biases in L1 are higher than in L2 (0.44°–0.77 °C/m), which may be partially attributed to the significantly greater temporal variability of the temperature gradients near the glacier surface.

Furthermore, as illustrated in Figure 5, the temperature variances obtained from the turbulence sensors and the screen measurements indicate that the screen measurements exhibit smaller variances compared to the eddy-covariance sensors during certain periods. This discrepancy is most pronounced during katabatic flow conditions in the forenoon at a height of 1.1 m above ground. In contrast, under disturbed conditions and during nighttime katabatic flows, the temperature variances align

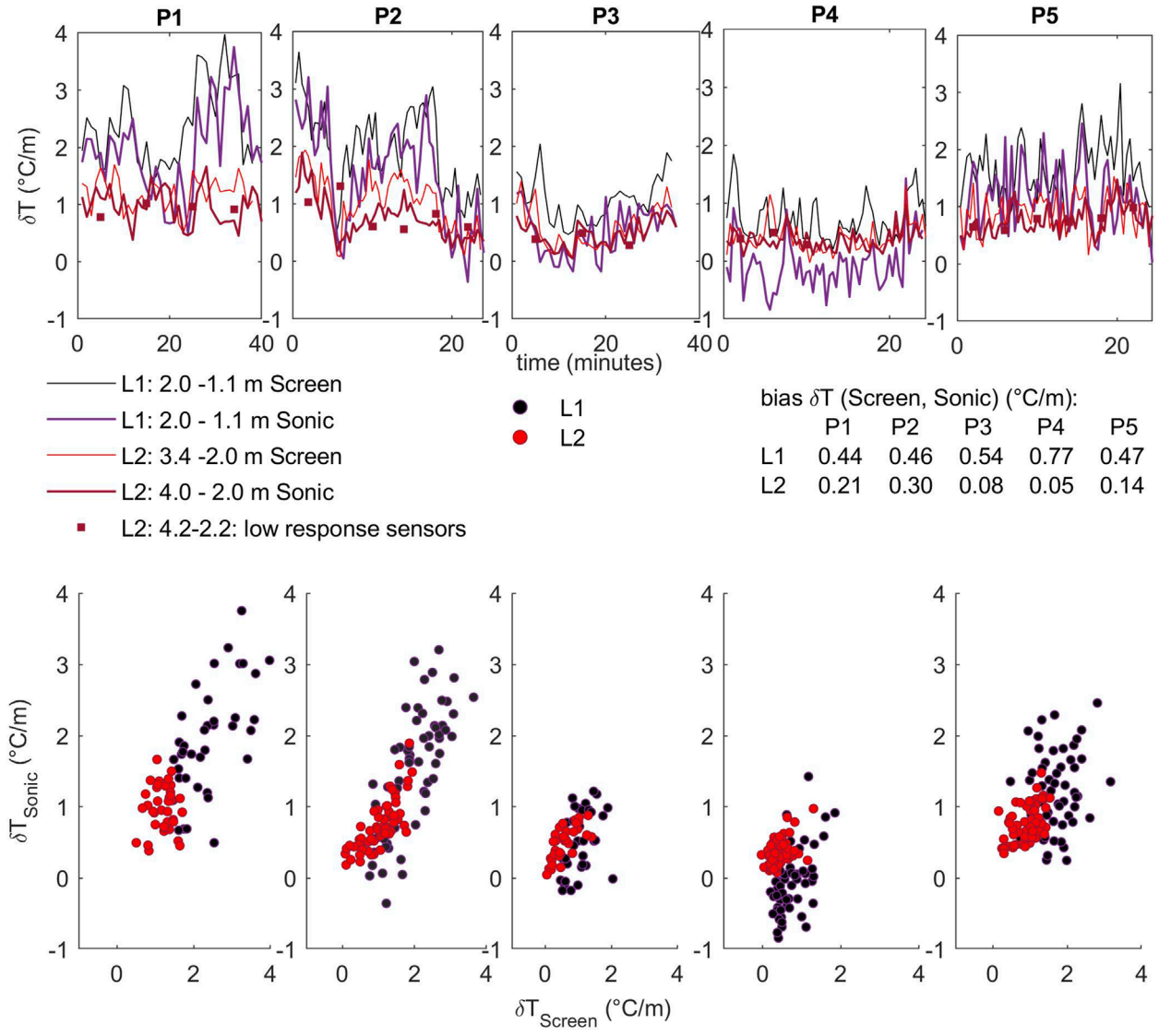

FIGURE 4
Time series (upper panels) and scatter plots (lower panels) of temperature gradients. Temperature gradients per meter were calculated between the second and first measurement levels (L1) and between the third and second levels (L2), using 1-min averaged temperatures. Data were obtained from screen and 3D sonic anemometers (IRGASON and CSAT3B). Note: Level L1 corresponds to heights of 1.1 m and 2.0 m above ground for both screen and sonic sensors, respectively. The maximum height for screen measurements at L3 is 3.4 m, while the highest CSAT3B sensor was installed at 4.0 m. Temperature gradient biases between the screen and sonic measurements are listed.

TABLE 1 Biases and correlation coefficients (*R*) between screen temperatures and low-frequency temperatures at sensor heights S2 (2.2 m) and S3 (4.2 m) above surface, separated by wind direction, daytime and nighttime conditions, and subperiods P1–P5.

Biases	Katabatic	Disturbed	Day	Night	P1	P2	P3	P4	P5
S2 (2.2m)	+0.7	−0.10	+1.6	−0.7	+0.9	+1.9	+1.5	−0.9	−0.5
S3 (4.2m)	+0.5	−0.6	+1.4	+1.2	+0.5	1.9	1.4	−1.6	−0.9
R	Katabatic	Disturbed	Day	Night					
S2 (2.2m)	0.97	0.86	0.81	0.80					
S3 (4.2m)	0.97	0.89	0.5	0.68					

Note that *R* values were not calculated for the subperiods due to the limited number of low-frequency measurements within these short time intervals.

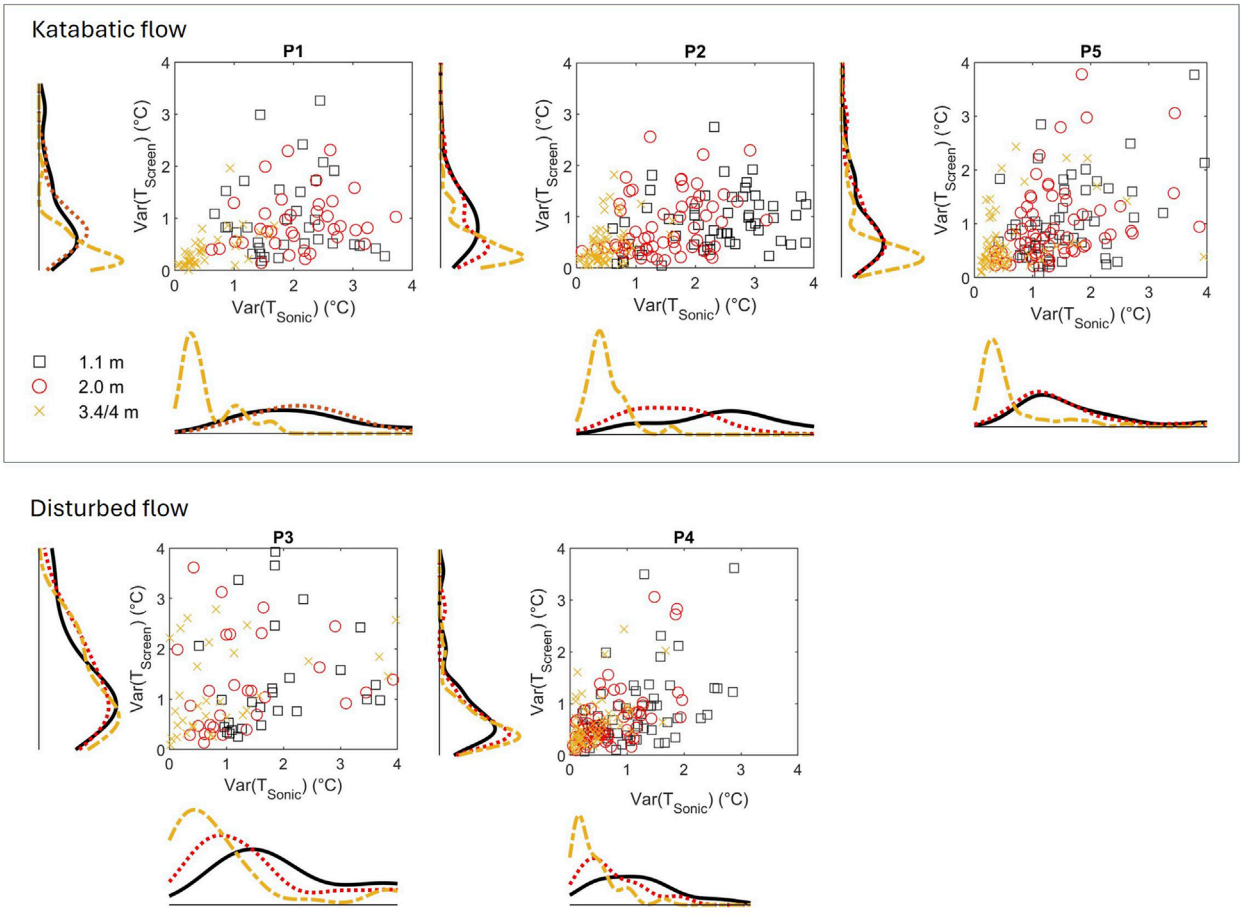

FIGURE 5
Scatter plots and histograms for temperature variance measured at the screen and the tower at three different heights. Temperature variances are shown for katabatic flow situations (P1, P2, P5) and distrubed flow conditions (P3, P4).

closely between screen and station measurements, demonstrating consistency in these specific periods. Furthermore, variances are well captured at higher levels, between 2 m and 4 m above ground. This may be partly attributed to the more dynamic temperature environment at 1.1 m, where temperature fluctuations are more intense, whereas higher levels experience less pronounced high-frequency temperature fluctuations.

This comparison underscores that the screen TIR method tends to underestimate particularly high temperature variances, although it reliably captures relative differences between variances across different heights. The variance underestimate is more pronounced during specific situations, while it aligns well during other periods. These findings may reflect slight differences in flow conditions between the screen and station locations, particularly as the jet height varies significantly over time, potentially influencing temperature fluctuations at specific heights. The temporal dynamics of temperature fluctuations over the entire profile is discussed in Section 3.3.

The slight underestimation of high-frequency temperature fluctuations suggests that the screen material's thermal response may be too slow to accurately resolve ultra-high frequencies, such as those at 30 Hz. To evaluate the frequency response of the TIR-based screen temperature measurements, we computed temperature spectra (seen in Figure 6) for three heights above the surface (1.1 m, 2 m, and 3.4/4 m) during three distinct observational periods: a katabatic day (P1), a mostly katabatic day (P2), and a katabatic night (P5). Spectra derived from screen temperature data (blue curves) were compared to those from co-located sonic temperature measurements (red curves), with a reference −2/3 slope line included to represent the expected behavior in the inertial subrange. At all heights and across all periods, the screen-derived spectra closely followed the sonic temperature spectra very well up to approximately 0.1 Hz, indicating that low-frequency temperature fluctuations are well captured by the TIR method. However, at higher frequencies (> 0.1 Hz), the screen spectra diverged notably, exhibiting a steeper slope than the canonical −2/3, consistent with the behavior of a low-pass filter. This deviation suggests that the thermal inertia or slow response time of the screen material limits its ability to resolve rapid temperature fluctuations. As a result, high-frequency variability—particularly in the inertial subrange—is attenuated, leading to an underestimation of small-scale turbulent processes. These findings highlight the utility of the TIR method for capturing mesoscale temperature variability while also underscoring its limitations in representing

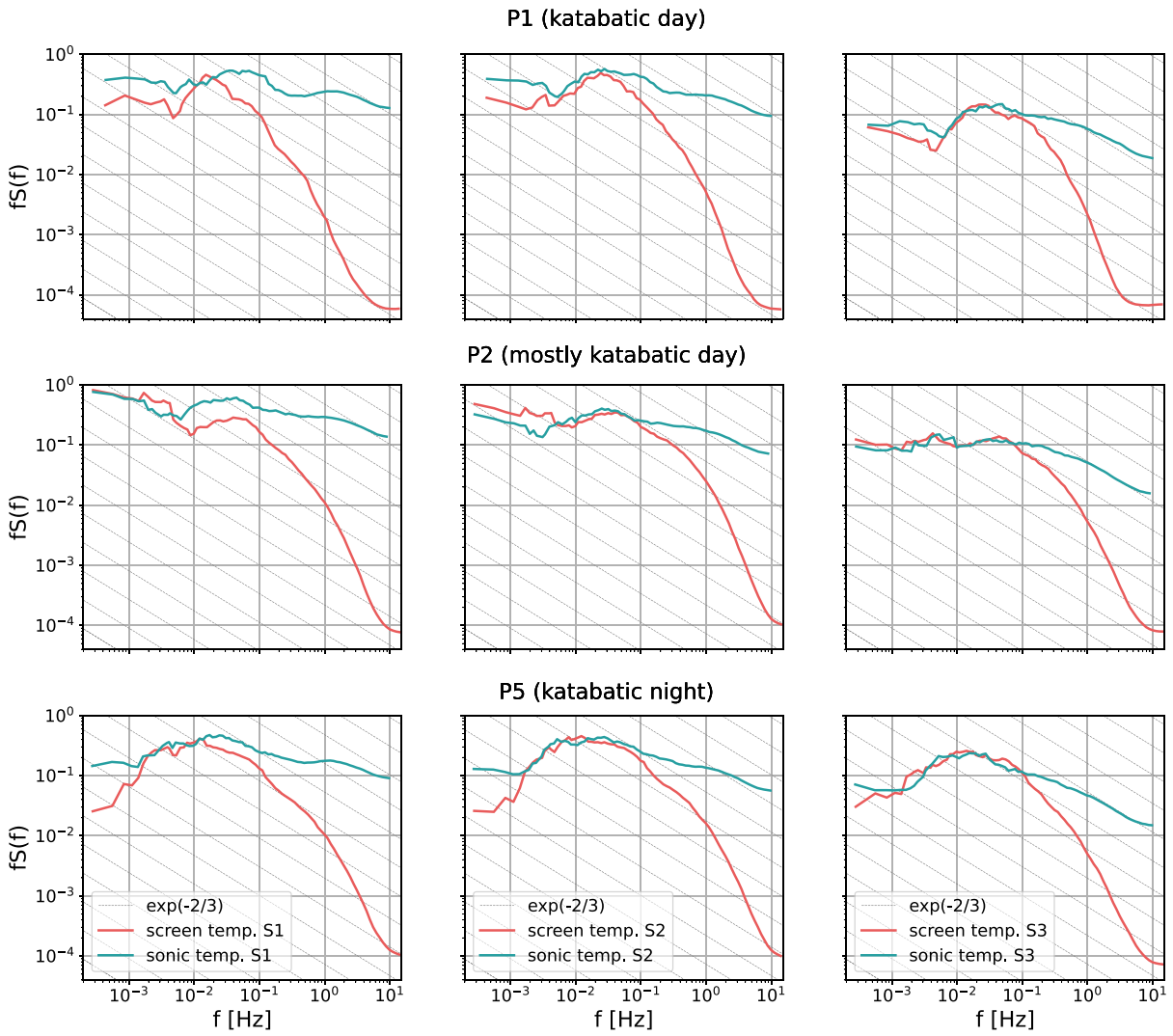

FIGURE 6
Temperature spectra at different heights above the surface for katabatic flow situations, periods P1, P2, and P5. The blue lines represent spectra derived from sonic temperature measurements at sensor levels S1 (1.1 m), S2 (2 m), and S3 (4 m), while the red lines correspond to screen temperature data at S1 (1.1 m), S2 (2 m), and S3 (3.4 m, the maximum height of screen measurements). The dotted lines indicate the −2/3 slope characteristic of the inertial subrange.

high-frequency fluctuations critical for characterizing atmospheric turbulence.

3.3 Air temperature dynamics close to the glacier surface

3.3.1 Comparison of katabatic flows and disturbed situations: vertical temperature profiles

Temperature profiles measured at the screen with 30 Hz were averaged over 5 min intervals and are presented for various wind conditions: glacier winds during the day (P1) and night (P5) (Figure 7), partially disturbed glacier winds (P2), and across-glacier winds (P3 and P4) (Figure 8). Additionally, we show the variance of screen temperature during 5-min sequences, indicating temperature variations and the mixing of warmer and colder air plumes at specific heights above the glacier surface. It should be noted that the screens do not align perfectly with the mean wind direction during disturbed flow conditions, potentially leading to measurement artifacts by flow blocking. However, we hypothesize that these artifacts are mitigated by smaller wind velocities and varying wind directions (Figure 1) during these conditions. Furthermore, temperature profiles are averaged over 5 min.

Measurements reveal lower temperatures near the glacier surface during katabatic winds than disturbed conditions, with mean temperature profiles exhibiting a steeper vertical gradient. For P1, this gradient is especially pronounced near the surface, showing temperature differences of 4 °C–5 °C within the lowest 2 m and approximately 2 °C difference between 2 and 3.5 m. For P5, glacier wind during night, the temperature gradient is slightly smaller with approx. 4 °C for the entire profile. Temperature variances for katabatic winds indicate enhanced temperature variation in

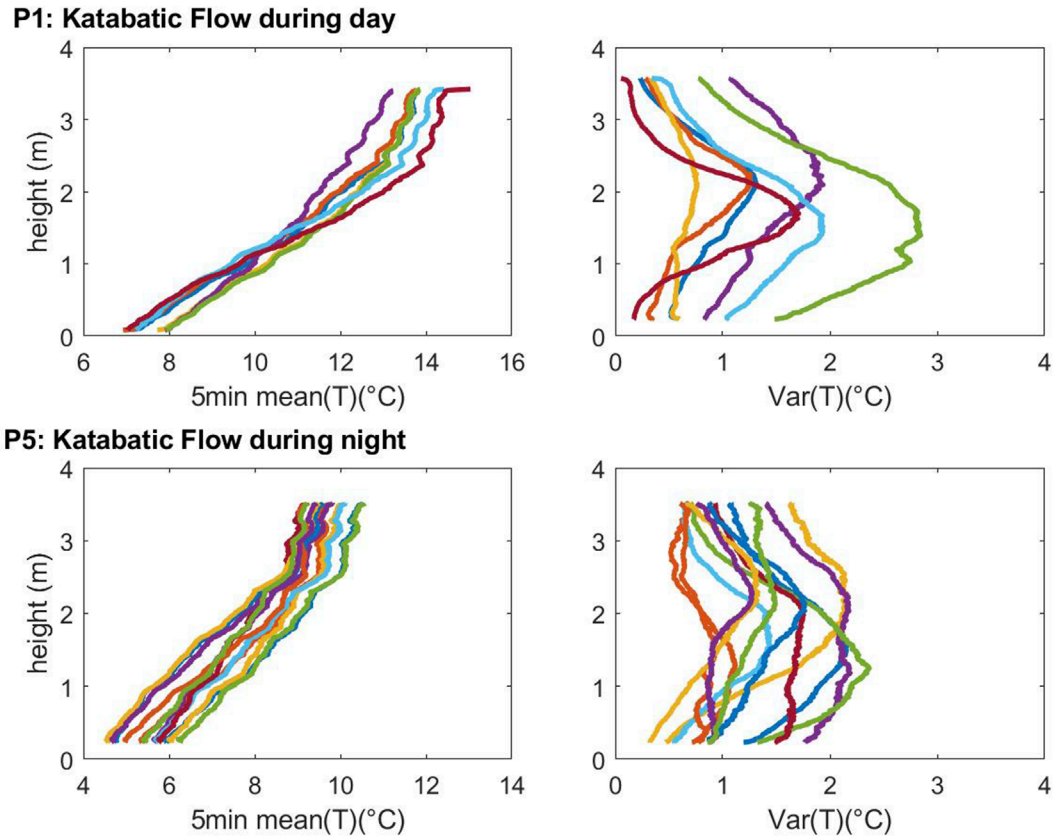

FIGURE 7
Profiles of screen temperatures and temperature variances averaged over 5-min intervals for katabatic flow conditions during day (P1) and night (P5).

atmospheric layers between approximately 1 and 3 m above the ground. This suggests that the strongest mixing of warm and cold air plumes, potentially advected from upstream, occurs at these atmospheric layers. The variance of temperature is much smaller, close to the surface, particularly for P1, indicating less mixing of warmer air masses within the first meter above the glacier surface. During glacier wind conditions in the night, the temporal temperature variance is smaller than during the day and maximum variances are less restricted to certain atmospheric layers.

Under disturbed conditions, the mean air temperature profiles exhibit much smaller temperature gradients, with temperature differences of only 2 °C–3 °C within the first 3.5 m above the ground. However, the variability between the mean temperature profiles is significantly greater for disturbed conditions compared to katabatic flows, indicating more pronounced fluctuations in flow conditions. This increased variability is further supported by the temperature variances within individual profiles, which are consistently strong throughout the entire vertical profile, unlike in katabatic flows where such variances are typically confined to specific atmospheric layers. This suggests enhanced air mixing across the entire profile, particularly in the lowest layers near the surface, where the 5-min temperature variance is highest. These findings indicate that during disturbed conditions, warm air is actively entrained and mixed downward toward the glacier surface, leading to significantly elevated near-surface air temperatures and less stable temperature profiles. In some cases, particularly high variances are observed very close to the surface, potentially caused by flow blocking and updraft near the ground caused by the screen.

3.3.2 Characterizing the glacier wind with temporally highly resolved temperature data during strong katabatic situations

Temperature dynamics exhibited strong vertical gradients during periods P1 and P5, when katabatic flows were most pronounced in the morning and nighttime hours. Screen temperature profiles, averaged over 1-s and 1-min intervals, are presented for 5-min subperiods (P1A–P1H, P5A–P5H) in Figure 9, offering a highly temporally resolved view of temperature variation.

As shown in the 5-min averaged profiles (Figure 7), steep temperature gradients consistently occur near the surface, transitioning to a more weakly stratified layer above. A closer examination reveals a more nuanced vertical structure during daytime katabatic flows (e.g., $P1_A$, $P1_C$, $P1_F$, $P1_G$), where the strongest gradients typically appear between approximately 1 m and 2.5 m. In contrast, gradients near the surface and at higher levels tend to be less steep during these periods. At night, subperiods such as $P5_D$, $P5_F$, and $P5_H$ also show distinct layers with strong gradients between 1 and 2.5 m above the glacier surface. In some cases, a clear break in stratification occurs above 2.5 m, suggesting a transition to a different temperature or flow regime.

High resolution 1-s profiles highlight that temperature variability is not uniform across all periods. Variations are generally

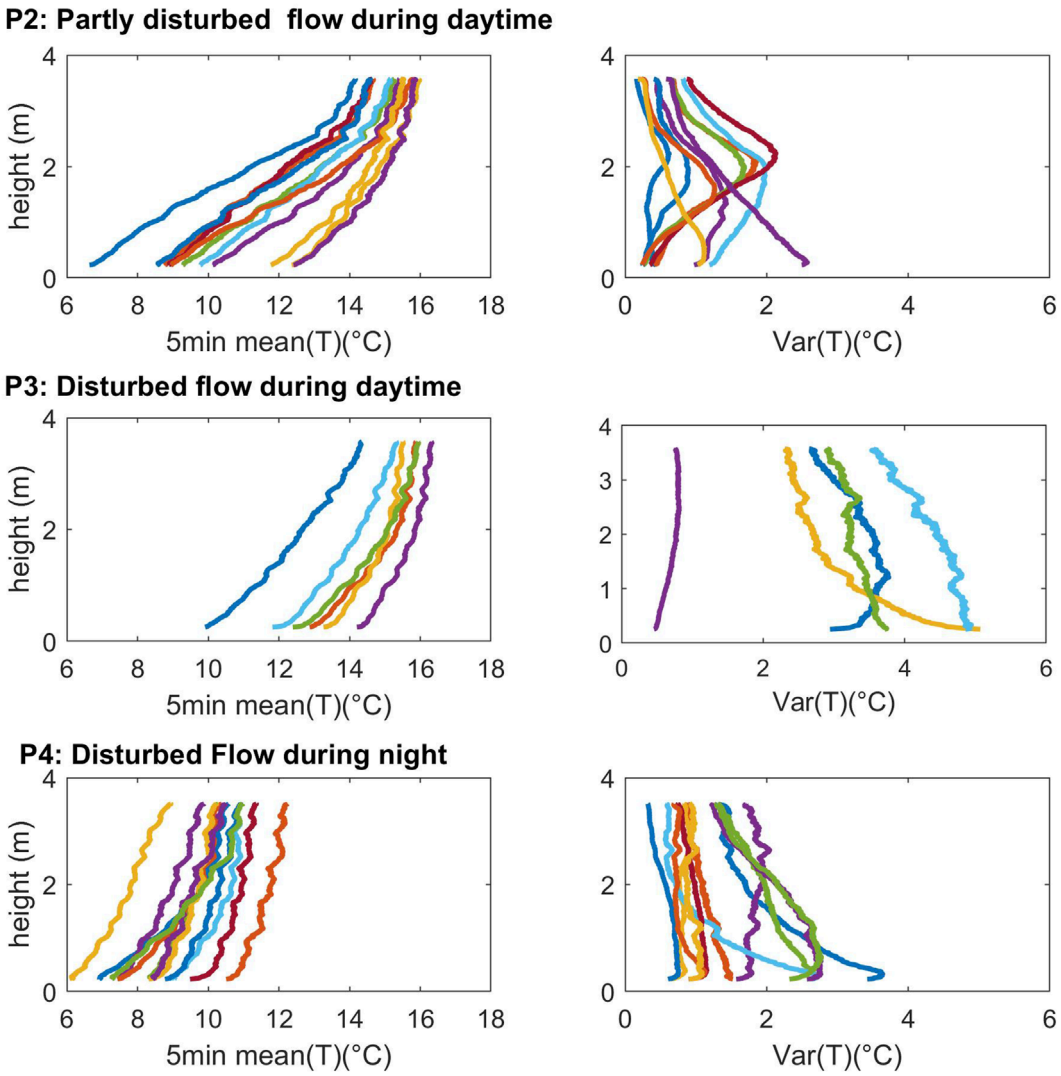

FIGURE 8
Profiles of screen temperatures and temperature variances averaged over 5-min intervals for disturbed flow conditions during day (P3) and night (P4) and for party disturbed conditions during the day (P2).

more pronounced at night compared to daytime glacier wind conditions. During daytime flows, some subperiods (e.g., $P1_A$, $P1_C$, and $P1_G$) show temporally consistent profiles, particularly at lower levels, indicating a persistent glacier wind. In contrast, subperiods such as $P1_E$ and $P1_F$ exhibit greater temporal variability, indicating more unstable or fluctuating wind conditions.

To further investigate the relationship between temperature stratification, temperature variance and glacier wind dynamics, Figures 10, 11 illustrate temperature variance profiles for 1-s and 1-min intervals. Furthermore, profiles of 1-min averages of streamwise heat flux ($u'T'$) and mean wind velocity, measured at three vertical levels at tower T275, approximate the vertical location of the jet height (Mott et al., 2020). Low-level jet turbulence profiles typically show a sign change in the streamwise heat flux (positive below and negative above) at the maximum wind speed (Grachev et al., 2016), allowing jet height estimation via interpolation between measurement points (Figures 10, 11E–H,Q-t).

Temperature variance profiles reveal that during certain periods (e.g., $P1_A$, $P1_B$, $P1_G$, and $P1_H$), the strongest variations occur between 1 and 3 m above the ground—coinciding with the region of steepest temperature gradients (Figure 9). Above this layer, where the stratification becomes weaker, temperature variance also decreases. Within the lowest meter, where temperatures remain cold and gradients are less steep (Figures 9a,b,f,g), temperature variations are minimal. This suggests a strong decoupling between the near-surface air and the layers above, limiting downward mixing of warmer air toward the glacier surface.

Turbulence profiles indicate that the jet height is most frequently located between 1 and 3 m above the glacier surface, though it occasionally drops below 1 m (e.g., $P1_D$ and $P1_E$), as supported by wind measurements. In periods where strong temperature variations are confined to the 1–3 m layer (e.g., $P1_A$, $P1_B$, and $P1_G$), the estimated jet height aligns well with these fluctuations, although some uncertainty in its estimation remains. Lower jet heights

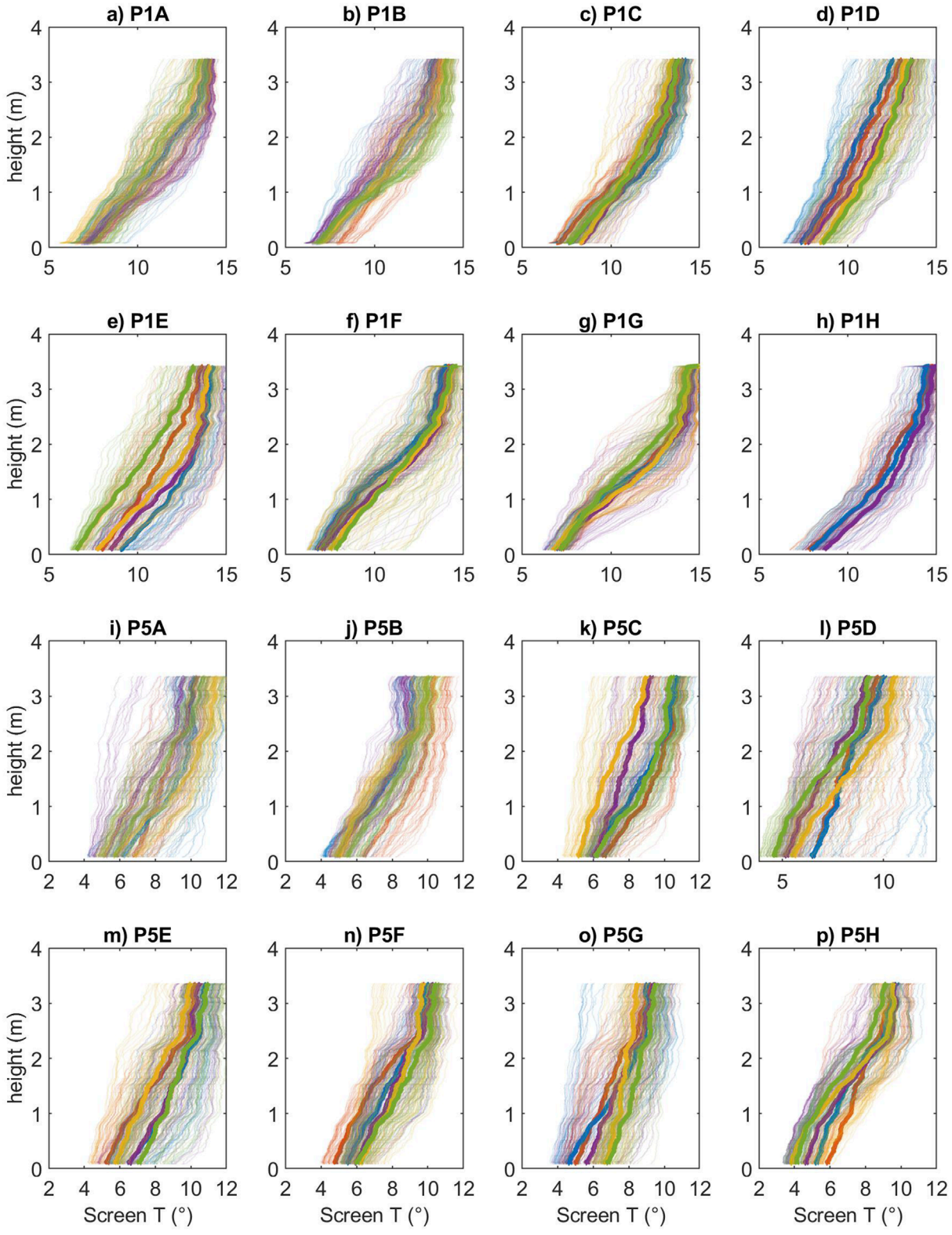

FIGURE 9
Profiles of Screen temperatures averaged over 1 s (thin lines) and 1 min (solid lines) intervals for 5 min intervals during strong katabatic flow situations in the morning (P1A-H) **(a–h)** and during the night (P5A-H) **(i–p)**. Note that the colour code used for the 1-min averages profile lines are the same as shown in Figure 10.

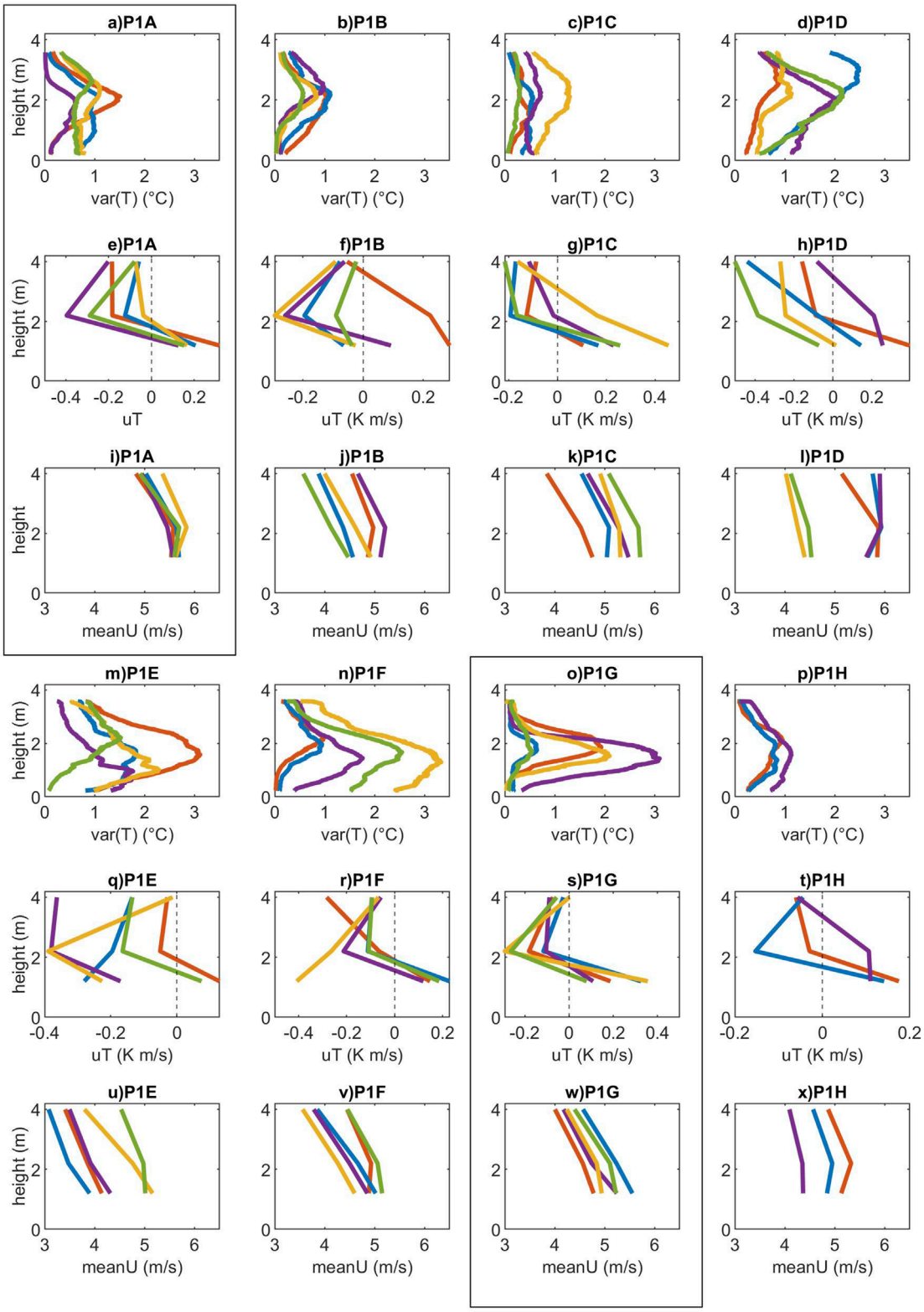

FIGURE 10
Profiles of Screen temperature variance 1 min intervals for 5 min intervals **(a–h)** during strong katabatic flow situations in the morning (P1) **(a,b,d,c,m,n,o,p)**. Corresponding profiles of 1 min averaged stream-wise heat flux (u'T') **(e,f,g,h,q,r,s,t)** and mean wind speed (meanU) **(i,j,k,l,u,v,w,x)** measured at the tower are shown as well.

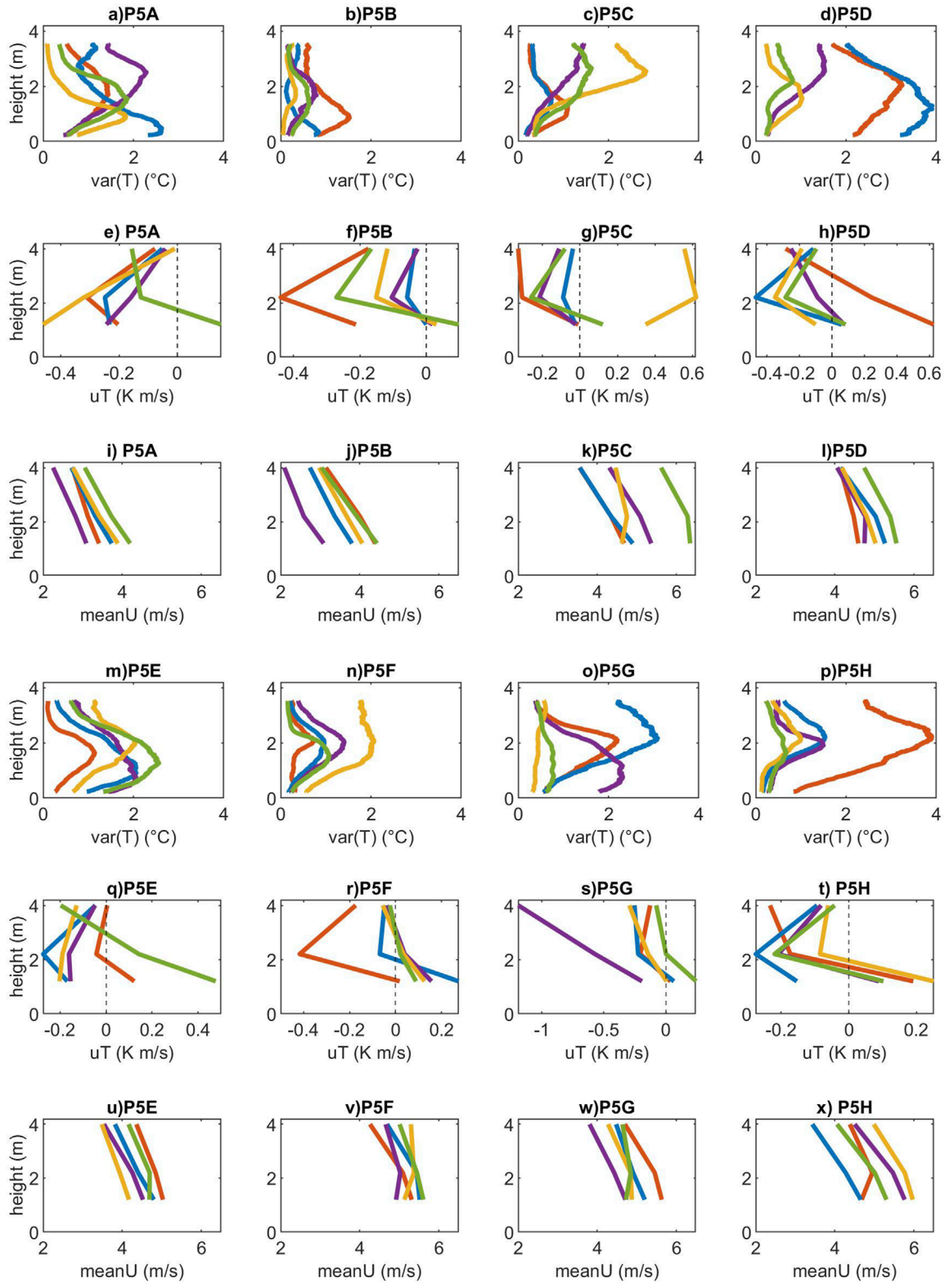

FIGURE 11
Profiles of Screen temperature variance over 1 min intervals for 5 min intervals during strong katabatic flow situations in the night (P5) **(a,b,d,c,m,n,o,p)**. Corresponding profiles of 1 min averaged stream-wise heat flux (uT) **(e,f,g,h,q,r,s,t)** and mean wind speed (meanU) **(i,j,k,l,u,v,w,x)** measured at the tower are shown as well.

correspond to increased temperature variability near the surface. Moreover, during periods such as $P1_A$ and $P1_G$, where the height of maximum temperature variance is well-defined, the jet height also remains temporally more stable, supporting the presence of a persistent katabatic flow.

In contrast, some periods (e.g., $P1_F$) exhibit strong temperature variations at the lowest 1 m above the glacier surface, suggesting intermittent entrainment of warm air into lower atmospheric layers and enhanced heat transport to the glacier surface. $P1_E$ and $P1_F$ are also characterized by lower jet heights and highly variable wind speed profiles, indicating less persistent wind conditions. For specific periods (e.g., $P1_A$, $P1_C$, $P1_F$, and $P1_G$), jet heights remain consistently below 2 m, aligning well with distinct changes in temperature stratification. Conversely, during periods such as $P1_D$, $P1_E$, and $P1_H$, streamwise momentum flux profiles show less distinct jet heights, with either negative or positive values across all three measurement heights or highly variable jet heights over time. These profiles suggest that measurement heights are either above (positive values) or below (negative values) the jet height, leading to more diffuse temperature variation across the profile without a clear layer of maximum fluctuation. This variability implies that flow conditions during these periods fluctuated between shallow and deep glacier winds, explaining why, in some cases, temperature variation—indicating cold and warm air mixing—is even stronger in layers adjacent to the glacier surface than above. During the nighttime katabatic flow (P5), temperature variance profiles reveal distinct atmospheric layers with pronounced fluctuations. However, these patterns are generally less temporally stable compared to the morning katabatic flow (P1). Certain subperiods, such as P5G and P5H, exhibit strong temperature variance between 1 and 3 m, coinciding with jet height estimates. However, in some cases, the strongest temperature variance occurs either below or above the estimated jet height, making it difficult to establish a definitive relationship between temperature fluctuations and jet height.

Although we found interesting correlations between temperature stratification, temperature variance and jet height estimates, it remains unclear whether the strongest temperature variations occur precisely at the glacier jet height, below, or above the maximum wind speed. Further turbulence and IR data investigations are needed to fully understand the interplay between glacier wind dynamics and the mixing of warm air toward the glacier surface. However, preliminary data suggest that near-surface temperature variations, indicating strong mixing of air close to the surface, are more pronounced in situations with shallow glacier winds. In contrast, temperature variations appear much smaller, indicating weaker air movement close to the glacier surface when glacier winds increase in depth. These high-resolution measurements support a finding by Mott et al. (2020), who showed that the evolution of the across-glacier flow also coincided with increasing turbulence from the peripheral zone towards the center line, promoting turbulent heat exchange towards the glacier surface.

4 Conclusion

We presented ultra-high-resolution thermal infrared data capturing temperature dynamics within the first meters above the glacier surface. These measurements complement turbulence observations, offering a detailed view of near-surface thermal processes driven by glacier winds. Our results show that stable atmospheric layers frequently form near the surface but are intermittently disrupted by warm-air advection, underscoring their importance for the glacier's energy balance.

Combining thermal and turbulence data revealed that during glacier winds, temperature variability and strong gradients are confined to layers near the glacier-wind jet height. When cross-glacier flows disrupt these winds, turbulence increases, enhancing warm-air mixing and weakening stratification. These patterns align with Mott et al. (2020), who found that cross-glacier flows disrupt katabatic winds and enhance turbulent heat exchange despite weaker near-surface winds.

Our high-resolution measurements extend this understanding by directly resolving how turbulence structures shape fine-scale thermal variability in the lowest atmospheric layers. The data provide new insight into the links between jet height, warm-air entrainment, and near-surface thermodynamics.

Profiles of temperatures, variances, and jet height estimates from turbulence data reveal certain relationships between temperature stratification, air temperature mixing, and jet height:

1. Temperature Stratification and Variance: Strong near-surface temperature gradients occur during katabatic flow, transitioning to weaker stratification above. A frequent break between 2 and 3 m separates distinct flow regimes. The steepest gradients (1–2.5 m) closely align with the height of maximum temperature variance.
2. Temperature Variance and Jet Height: Jet heights commonly range between 1 and 3 m, occasionally below 1 m. Temperature variance peaks within similar layers, though correlation is limited by exact jet height uncertainty. Persistent katabatic flow produces stable variance heights, while fluctuating jets yield broader, less defined variance layers. Lower jet heights correspond to stronger near-surface temperature variations, indicating enhanced downward mixing.
3. Near-Surface Dynamics: Periods of high variance within the lowest meter above surface indicate intermittent warm-air entrainment and enhanced heat transport within the atmospheric layers adjacent to the glacier surface. Near-surface temperature variations intensify during shallow glacier winds and weaken during deeper flows.
4. Implications of Temperature Variance and Jet Height Relationships: The alignment of the approximate jet height and maximum temperature variance underscores the role of katabatic flow in controlling stratification and atmospheric mixing. Stable regimes show strong coupling between jet height and variance, while fluctuating flows weaken this relationship, reflecting complex near-surface dynamics.

Although relationships between temperature stratification, temperature variance, and jet height were evident, the link between the strongest temperature variations and jet height remains uncertain. Further work combining turbulence and IR data is needed to clarify glacier-wind dynamics and their role in warm-air mixing near the surface. Adapting the

WEIRD method (Haugeneder et al., 2023) to glacier-wind conditions, together with heat-budget analysis, will help refine this understanding. Still, our results suggest that shallow glacier winds enhance near-surface temperature variations, whereas deeper flows suppress mixing.

Limitations and uncertainties remain regarding screen temperatures derived from the TIR camera. Measurements at different heights can be affected by wind speed, surface longwave radiation (including reflected solar radiation), and direct solar radiation, with their influence depending on the solar angle of incidence.

Despite these limitations, the methods and findings presented here offer new opportunities for studying microscale temperature dynamics in the near-surface atmosphere. Integrating high-resolution thermal imaging with turbulence measurements provides a powerful framework for resolving fine-scale structures, stable stratification, and cold-air pooling. This approach is applicable to other glacierized, mountainous, or basin environments where drainage flows and air-mass advection shape surface–atmosphere exchanges, and can support improved parameterization of stable boundary layers and surface energy fluxes in high-resolution weather and climate models.

Data availability statement

The thermal infrared data analysed in this study is available from the Zenodo repository: 10.5281/zenodo.15792038.

Author contributions

RM: Formal Analysis, Supervision, Writing – original draft, Methodology, Resources, Data curation, Software, Visualization, Project administration, Conceptualization, Writing – review and editing, Investigation, Validation, Funding acquisition. MH: Formal Analysis, Writing – original draft, Data curation, Methodology, Writing – review and editing. IS: Conceptualization, Writing – original draft, Methodology, Writing – review and editing, Funding acquisition, Data curation. PA: Formal Analysis, Writing – original draft, Methodology, Investigation, Writing – review and editing. DR: Writing – review and editing, Writing – original draft, Conceptualization, Methodology. LN: Writing – original draft, Investigation, Funding acquisition, Project administration.

Funding

The authors declare that financial support was received for the research and/or publication of this article. The authors thank the funding source of this project, the Swiss National Science Foundation grant *The microclimate on glaciers*, grant number #219918. The field work was further supported by the Transnational Access from the European Union's H2020 project INTERACT III, under grant agreement #871120. The research of I. Stiperski received funding from the European Research Council (ERC) under the European Union's Horizon 2020 research and innovation program (Grant agreement No. 101001691).

Acknowledgements

The authors thank researchers involved in the HEFEX II field campaign, particularly Rainer Prinz, Alexander Georgi, Alexander R. Groos, Thomas E. Shaw, Tobias Sauter, Jean-Emmanuel Sicart, Ben W. Brock, Roland Albers, Balthazar Allegri, Helene Barral, Claudine Charrondiere, Catherine Coulaud, Alexander Fischer, Niklas Richter, Marie Schroeder, Phillip Vettori, Annelies Voordendag and Carlos Wydra.

Conflict of interest

The authors declare that the research was conducted in the absence of any commercial or financial relationships that could be construed as a potential conflict of interest.

The author(s) declared that they were an editorial board member of Frontiers, at the time of submission. This had no impact on the peer review process and the final decision.

Generative AI statement

The authors declare that no Generative AI was used in the creation of this manuscript.

Any alternative text (alt text) provided alongside figures in this article has been generated by Frontiers with the support of artificial intelligence and reasonable efforts have been made to ensure accuracy, including review by the authors wherever possible. If you identify any issues, please contact us.

Publisher's note

References

Abermann, J., Lambrecht, A., Fischer, A., and Kuhn, M. (2009). Quantifying changes and trends in glacier area and volume in the Austrian Ötztal Alps (1969-1997-2006). *Cryosphere* 3, 205–215. doi:10.5194/tc-3-205-2009

Brock, B., Rivera, A., Casassa, G., Bown, F., and Acuña, C. (2007). The surface energy balance of an active ice-covered volcano: Villarrica Volcano, southern Chile. *Ann. Glaciol.* 45, 104–114. doi:10.3189/172756407782282372

Chambers, J. R., Smith, M. W., Smith, T., Sailer, R., Quincey, D. J., Carrivick, J. L., et al. (2021). "Correcting for systematic underestimation of topographic Glacier aerodynamic roughness values from Hintereisferner, Austria," *Front. Earth Sci. (Lausanne)*. 9. 691195. doi:10.3389/feart.2021.691195

Conway, J., and Cullen, N. (2013). Constraining turbulent heat flux parameterization over a temperate maritime glacier in New Zealand. *Ann. Glaciol.* 54, 41–51. doi:10.3189/2013AoG63A604

Conway, J., Abermann, J., Andreassen, L. M., Azam, M. F., Cullen, N. J., Fitzpatrick, N., et al. (2022). Cloud forcing of surface energy balance from *in situ* measurements in diverse mountain glacier environments. *Cryosphere* 16, 3331–3356. doi:10.5194/tc-16-3331-2022

Denby, B. (1999). Second-order modelling of turbulence in katabatic flows. *Boundary-Layer Meteorol.* 92, 65–98. doi:10.1023/A:1001796906927

Fitzpatrick, N., Radić, V., and Menounos, B. (2017). Surface energy balance closure and turbulent flux parameterization on a mid-latitude mountain glacier, Purcell mountains, Canada. *Front. Earth Sci.* 5, 67. doi:10.3389/feart.2017.00067

Frei, C., and Schär, C. (1998). A precipitation climatology of the alps from high-resolution rain-gauge observations. *Int. J. Climatol. A J. R. Meteorological Soc.* 18, 873–900. doi:10.1002/(SICI)1097-0088(19980630)18:8<873::AID-JOC255>3.0.CO;2-9

Goger, B., Stiperski, I., Nicholson, L., and Sauter, T. (2022). Large-eddy simulations of the atmospheric boundary layer over an Alpine glacier: impact of synoptic flow direction and governing processes. *Q. J. R. Meteorological Soc.* 148, 1319–1343. doi:10.1002/qj.4263

Goger, B., Stiperski, I., Ouy, M., and Nicholson, L. (2025). Investigating the influence of changing ice surfaces on gravity wave formation impacting glacier boundary layer flow with large-eddy simulations. *Weather Clim. Dyn.* 6, 345–367. doi:10.5194/wcd-6-345-2025

Grachev, A. A., Leo, L. S., Sabatino, S. D., Fernando, H. J. S., Pardyjak, E. R., and Fairall, C. W. (2016). Structure of turbulence in katabatic flows below and above the wind-speed maximum. *Boundary-Layer Meteorol.* 159, 469–494. doi:10.1007/s10546-015-0034-8

Grudzielanek, A. M., and Cermak, J. (2015). Capturing cold-air flow using thermal imaging. *Boundary-Layer Meteorol.*, 157. doi:10.1007/s10546-015-0042-8

Haugeneder, M., Lehning, M., Reynolds, D., Jonas, T., and Mott, R. (2023). A novel method to quantify near-surface boundary-layer dynamics at ultra-high spatio-temporal resolution. *Temporal Resolut.* 186, 177–197. doi:10.1007/s10546-022-00752-3

Haugeneder, M., Lehning, M., Stiperski, I., Reynolds, D., and Mott, R. (2024). Turbulence in the strongly heterogeneous near-surface boundary layer over patchy snow. *Bound. Layer. Meteorol.* 190, 7. doi:10.1007/s10546-023-00856-4

Hock, R. (2005). Glacier melt: a review of processes and their modelling. *Prog. Phys. Geogr. Earth Environ.* 29, 362–391. doi:10.1191/0309133305pp453ra

Hoinkes, H. (1954). Beiträge zur Kenntnis des Gletscherwindes. *Arch. für Meteorol. Geophys. Bioklimatol. Ser. B* 6, 36–53. doi:10.1007/bf02246739

Klug, C., Bollmann, E., Galos, S. P., Nicholson, L., Prinz, R., Rieg, L., et al. (2018). Geodetic reanalysis of annual glaciological mass balances (2001–2011) of Hintereisferner, Austria. *Cryosphere* 12, 833–849. doi:10.5194/tc-12-833-2018

Kuhn, M., Dreiseitl, E., Hofinger, S., Markl, G., Span, N., and Kaser, G. (1999). Measurements and models of the mass balance of Hintereisferner. *Geogr. Ann. Ser. A Phys. Geogr.* 81, 659–670. doi:10.1111/1468-0459.00094

Mott, R., Wolf, A., Kehl, M., Kunstmann, H., Warscher, M., and Grünewald, T. (2019). Avalanches and micrometeorology driving mass and energy balance of thelowest perennial ice field of the Alps: a case study. *The Cryosphere* 13(4), 1247–1265. doi:10.5194/tc-13-1247-2019

Mott, R., Stiperski, I., and Nicholson, L. (2020). Spatio-temporal flow variations driving heat exchange processes at a mountain glacier. *Cryosphere* 14, 4699–4718. doi:10.5194/tc-14-4699-2020

Nicholson, L., Stiperski, I., Nitti, G., Prinz, R., Georgi, A., Groos, A. R., et al. (2025). The second hintereisferner experiment (hefex ii): initial insights into boundary layer structure and surface–atmosphere exchange processes from intensive observations at a valley glacier. *Bull. Am. Meteorological Soc.* 106, E2143–E2169. doi:10.1175/BAMS-D-24-0010.1

Obleitner, F. (1994). Climatological features of glacier and valley winds at the Hintereisferner (Ötztal Alps, Austria). *Theor. Appl. Climatol.* 49, 225–239. doi:10.1007/bf00867462

Oerlemans, J. (2001). *Glaciers and climate change*. CRC Press.

Sauter, T., and Galos, S. P. (2016). Effects of local advection on the spatial sensible heat flux variation on a mountain glacier. *Cryosphere* 10, 2887–2905. doi:10.5194/tc-10-2887-2016

Sauter, T., Brock, B. W., Collier, E., Georgi, A., Goger, B., Groos, A. R., et al. (2025). Glacier-atmosphere interactions and feedbacks in high-mountain regions - a review. *Water Resour. Res.*

Shaw, T. E., Buri, P., McCarthy, M., Miles, E. S., Ayala, A., and Pellicciotti, F. (2023). The decaying near-surface boundary layer of a retreating alpine glacier. *Geophys Res. Lett.* 50, e2023GL103043. doi:10.1029/2023GL103043

Smeets, C. J. P. P., Duynkerke, P. G., and Vugts, H. F. (2000). Turbulence characteristics of the stable boundary layer over A mid-latitude Glacier. Part Ii: pure katabatic forcing conditions. *Boundary-Layer Meteorol.* 97, 73–107. doi:10.1023/A:1002738407295

Strasser, U., Marke, T., Braun, L., Escher-Vetter, H., Juen, I., Kuhn, M., et al. (2018). The Rofental: a high alpine research basin (1890–3770 m a.s.l.) in the Ötztal Alps (Austria) with over 150 years of hydrometeorological and glaciological observations. *Earth Syst. Sci. Data* 10, 151–171. doi:10.5194/essd-10-151-2018

Vickers, D., and Mahrt, L. (2003). The cospectral gap and turbulent flux calculations. *J. Atmos. Ocean. Technol.* 20, 660–672. doi:10.1175/1520-0426(2003)20<660:tcgatf>2.0.co;2